PNAS RESEARCH ARTICLE | BIOPHYSICS AND COMPUTATIONAL BIOLOGY

Emergent depth-mechanosensing of epithelial collectives regulates cell clustering and dispersal on layered matrices

Hongsheng Yu[a] and Amit Pathak[a,1]

Edited by Roberto Mayor, University College London, London, United Kingdom; received November 15, 2024; accepted August 11, 2025 by Editorial Board Member Yale E. Goldman

During wound healing, tumor growth, and organ formation, epithelial cells migrate and cluster in layered tissue environments. Although cellular mechanosensing of adhered extracellular matrices is now well recognized, it is unclear how deeply cells sense through distant matrix layers. Since single cells can mechanosense stiff basal surfaces through soft hydrogels of <10 μm thickness, here we ask whether cellular collectives can perform such "depth-mechanosensing" through thicker matrix layers. Using a collagen-polyacrylamide double-layer hydrogel, we found that epithelial cell collectives can mechanosense basal substrates at a depth of >100 μm, assessed by cell clustering and collagen deformation. On collagen layers with stiffer basal substrates, cells initially migrate slower while performing higher collagen deformation and stiffening, resulting in reduced dispersal of epithelial clusters. These processes occur in two broad phases: cellular clustering and dynamic collagen deformation, followed by cell migration and dispersal. Using a cell-populated collagen-polyacrylamide computational model, we show that stiffer basal substrates enable higher collagen deformation, which in turn extends the clustering phase of epithelial cells and reduces their dispersal. Disruption of collective collagen deformation, by either α-catenin depletion or myosin-II inhibition, disables the depth-mechanosensitive differences in epithelial responses between soft and stiff basal substrates. These findings suggest that depth-mechanosensing is an emergent property that arises from collective collagen deformation caused by epithelial cell clusters. This work broadens the conventional understanding of epithelial mechanosensing from immediate surfaces to underlying basal matrices, providing insights relevant to tissue contexts with layers of varying stiffness, such as wound healing and tumor invasion.

mechanobiology | extracellular matrix | collagen | mechanosensing | epithelial cells

Throughout essential biological processes of morphogenesis, aging, fibrotic diseases, regeneration, and repair, adherent cells reside in tissue contexts that vary in physical attributes such as geometry, stiffness, and topography (1–5). Over the past two decades, the ability of cells to sense the stiffness of their adhered extracellular matrix (ECM) has been widely appreciated, and such cellular mechanosensing regulates stem cell differentiation, proliferation, growth, migration, and various genetic and epigenetic transformations (6–9). Regardless of the tissue context, cellular mechanosensing of ECM stiffness fundamentally operates through active feedback between focal adhesions and actin–myosin contractile forces (10). Here, greater resistance from stiffer ECM strengthens receptor–ligand bonds through clustering of various focal adhesion proteins (e.g., vinculin, paxillin, talin), which in turn activate mechanosensing signaling pathways (e.g., Rho GTPases, Hippo) that aid actin–myosin stress fiber contractility (11). However, much of previous work considers the stiffness of surfaces immediately adhered to the cells, rather than the layered nature of tissue microenvironments. In vivo, cells often reside in layered microenvironments where the cell-adhered ECM may be soft, but that ECM could be attached to stiffer tissue layers. For instance, cells at the tumor–stromal interface could be attached to softer healthy tissue, which could be in close vicinity of a much stiffer tumor microenvironment, as these mechanical gradients can change within a few microns (12, 13); epithelial cells adhere to the basement membrane of submicron thickness that lines organ boundaries of distinct mechanical properties (14); osteoblasts adhere to a soft collagen-rich tissue layer that lines the much stiffer bone (15). Yet, it remains unclear and understudied how cells sense the mechanical properties of distant matrix layers that lie beyond the immediately adhered ECM.

Since matrix deformation fundamentally regulates cellular mechanosensing, soft but thin extracellular matrices could propagate their large deformations to stiffer basal tissue layers. As a result, such layered environments of soft ECM with a stiffer basal layer could provide an integrated stiff-like resistance for cellular forces and trigger cellular mechanotransduction

Significance

Previous work has shown that single cells can sense microenvironment stiffness through thin matrix layers, and this range extends with viscoelastic collagen compared to elastic hydrogels. Here, we found that epithelial cell collectives can mechanosense matrix stiffness over 100 μm deep into collagen layers. Stiffer basal matrix enables lower cell dispersal and higher clustering, enabled by collective collagen deformation and stiffening. According to our experiments and simulations, the inhibition of cellular contractility or intercellular adhesions disrupts this emergent phenomenon and disables depth mechanosensing. These findings expand the known length scales of conventional mechanosensing and suggest that cell clusters at tissue interfaces—such as in tumor invasion, wound healing, or organogenesis—mechanosense not only their adhered surfaces but also distant matrix layers.

Author affiliations: [a]Department of Mechanical Engineering and Materials Science, Washington University, St. Louis, MO 63130

Author contributions: H.Y. and A.P. designed research; H.Y. performed research; H.Y. contributed new reagents/analytic tools; H.Y. analyzed data; and H.Y. and A.P. wrote the paper.

The authors declare no competing interest.

This article is a PNAS Direct Submission. R.M. is a guest editor invited by the Editorial Board.

[1]To whom correspondence may be addressed. Email: pathaka@wustl.edu.

This article contains supporting information online at https://www.pnas.org/lookup/suppl/doi:10.1073/pnas.2423875122/-/DCSupplemental.

Published September 11, 2025.

pathways. Indeed, cells cultured on <1 μm thin and soft (<1 kPA) hydrogels spread significantly more than thick gels, because cells on thin gels can sense and respond to the rigid glass substrate underneath (16, 17). Here, displacements within softer gels propagate, and the presence of a glass surface underneath thin (~1 μm) gels increases interfacial strain and thus mechanosensing. Despite this early evidence, the extent of depth-mechanosensing for different cell types and ECM composition remains an open question (18). While previous studies have demonstrated that highly contractile cell types, such as fibroblasts and mesenchymal cells (18–20), generate forces that transmit over long distances, it remains unclear whether epithelial cells can pool their forces to generate long-distance force propagation. Building on this work, we recently showed that collagen layers that can be remodeled, unlike the linear elastic hydrogels, extend the length scale of depth-mechanosensing to ~10 μm, orchestrated through reciprocal feedback between cell polarity and collagen fiber remodeling (21).

Given the importance of polarized forces exerted by single cells in the generation of collagen deformations that penetrate through thin matrix layers (21), we next wondered whether cell collectives could integrate their forces and propagate collagen deformation even deeper and thus enhance the known length scales of depth-mechanosensing. Epithelial cells form multicellular clusters and monolayers to perform various fundamental biological functions, such as lining the organs, forming scars, and growing solid cancers (22, 23). In these processes, cells can also transmit and coordinate their forces to enable collective cell migration to enable wound healing and tumor invasion (23–25). These seemingly competitive processes of epithelial clustering and migration occur dynamically and autonomously according to biological demands and depending on ECM properties. Although epithelial cells are innately prone to coalesce into monolayers and clusters, stiffer ECMs trigger EMT-like responses wherein cells become elongated and migratory (26–28). As such, enhanced migration or dispersal of epithelial cells is associated with their mechanosensing of the adhered stiff substrates. To test the potential of depth-mechanosensing of epithelial collective, we measure their decision to cluster versus disperse on soft viscoelastic collagen layers adhered atop soft or stiff basal substrates. Here, we introduce an in vitro collagen-polyacrylamide (PA) double-layer system and show that depth-sensing of epithelial collectives gives rise to enhanced clustering and reduced cell migration, mediated by higher contractility, collagen deformation, and multicellular coordination. Through a cell-populated collagen-PA (CPCP) double-layer mathematical model, we delineate how depth-mechanosensing arises from relative forces and deformations in different matrix layers. These findings expand the known length scales of cellular depth-mechanosensing to ~100 μm, which was previously shown to be <5 μm for linear elastic matrices (16) and ~10 μm for collagen matrices (21) with single cells.

Results

Depth-Mechanosensing of Stiffer Basal Matrix Limits Dispersal of Grouped Epithelial Cells. To understand whether depth-mechanosensing of epithelial cells would affect their ability to cluster versus disperse on layered matrices, we sought a way to place a defined number of epithelial cells (MCF10A human mammary epithelial cell line) in consistent geometry (Fig. 1*A*). We fabricated PDMS microwells to pour colonies of 80 ± 18 cells on top of the collagen-polyacrylamide (col-PA) double-layer substrates (Fig. 1*A* and *SI Appendix*, Fig. S1*B*), with the top collagen layer of constant composition (1.3 mg/ml concentration and ~120 μm thickness, *SI Appendix*, Fig. S9*A*) but different basal PA stiffness (*SI Appendix*, Fig. S2*A*). This method of cell seeding

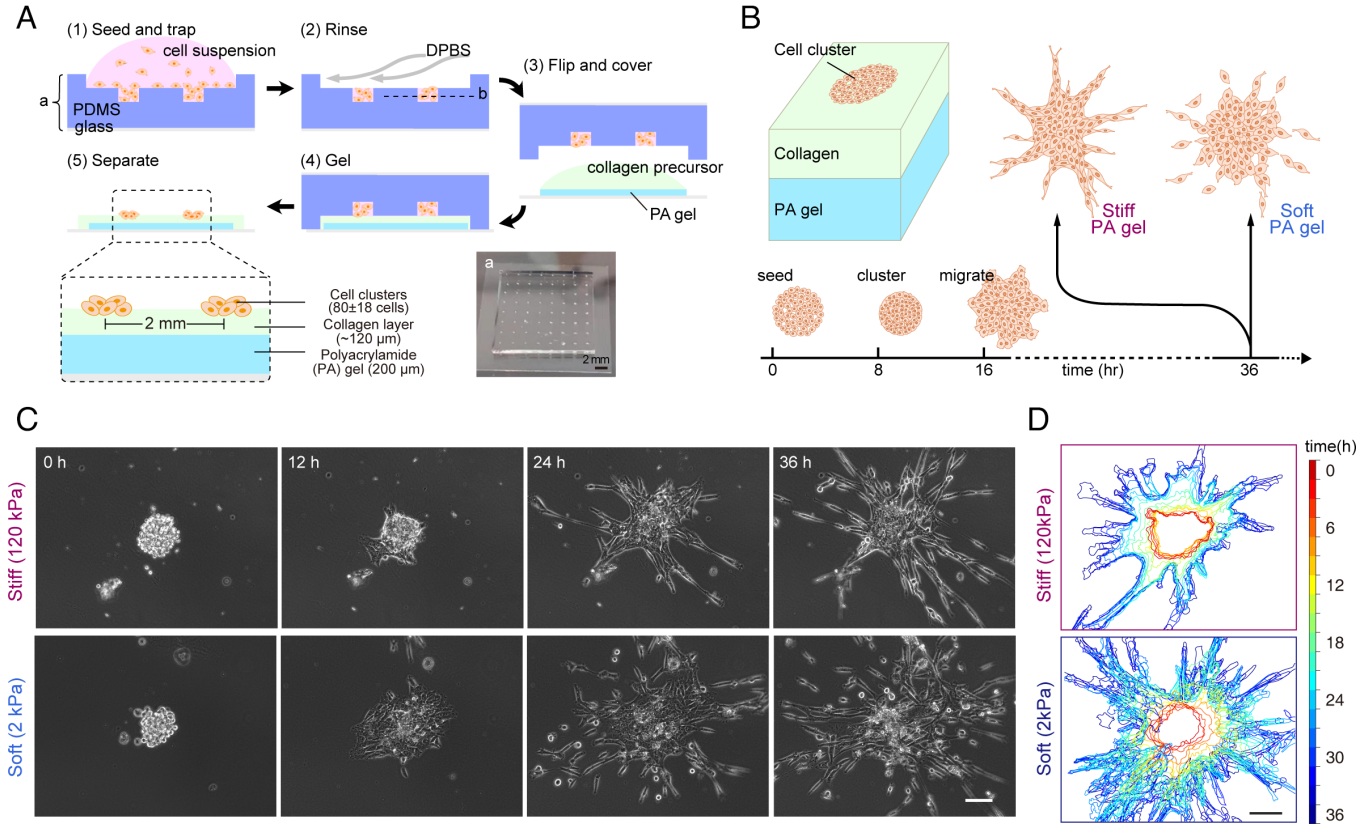

Fig. 1. Cell cluster formation on collagen-PA double-layer substrate. (*A*) Schematic of multicell cluster patterning on the collagen-PA substrate. (*B*) Schematic showing the representative cell cluster migration on col-PA double-layer substrate with different PA gel stiffness. (*C*) Brightfield image of cell cluster formation on col-PA substrate with different stiffness. (*D*) Cell cluster outline colored with time. (Scale bar, 100 μm.)

resulted in round ~150 μm diameter patterns of epithelial cells atop these double-layered matrices (Fig. 1*C*). We performed live time-lapse imaging and identified two phases of epithelial response—clustering followed by migratory dispersal (Fig. 1*B*). In the initial clustering phase, cells aggregate to form an epithelial cluster. While this clustering phase lasted ~8 h on collagen gels with a soft basal PA layer, a similar clustering process occurred for a longer duration (~12 h) with a stiff basal layer (Fig. 1*D* and Movie S1). Subsequently, during the cell migration phase, cell clusters started to expand and migrate outward from their initially seeded positions (Fig. 1 *C* and *D*).

To characterize how cells switch between migratory and clustering phenotypes on col-PA substrates with different basal layer stiffness, we visualized migration tracks of the fluorescence-labeled cells (Fig. 2*A*) as they moved outward from the initially seeded epithelial cell colony. Here, cell migration velocity peaked after ~12 h on collagen gels with soft basal matrix, thus entering the migration phase quickly. By contrast, cells slowly gained velocity for a longer duration on gels with a stiff basal layer and peaked after >20 h (Fig. 2*B*), which indicates their greater "depth-mechanosensitive" clustering potential. Here, although the cell migration velocity for the stiff basal layer was lower than the soft (Fig. 2*B*), both conditions yielded similar accumulated displacement after 20 h (Fig. 2*C*). We wondered whether this seemingly paradoxical relationship between slow speed and high displacement in the stiff group could be explained by their higher persistence. However, surprisingly, linear persistence of cell migration was lower (or comparable) for the stiff group (Fig. 2*D*). Since the clusters are roughly circular and cells are migrating radially outward, we characterize migratory persistence of cell migration in polar coordinates (Fig. 2*E*, radial persistence calculated as the cosine of the angle between position vector and cell migration velocity vector). A narrower distribution of cosθ close to 1 was found in the stiff group, indicating that cells in the stiff group have higher radial persistence (Fig. 2*E*), which is consistent with the longer and well-organized centrifugal cell migration trajectories (Fig. 2*A*). We found this depth-mechanosensitive clustering migration phenotype on collagen layers with stiffer basal substrate in another epithelial cell line, MDCK I (*SI Appendix*, Fig. S3 *A–D*), while cancerous cells (A431, *SI Appendix*, Fig. S3 *E–H*) and fibroblasts (CAFs, *SI Appendix*, Fig. S3 *I–L*) did not exhibit depth-mechanosensing.

To compare the epithelial clustering migration with the single cell migration, we seeded single MCF10A cells on our double-layer substrates. We found no significant difference in single cell migration with different basal PA gel stiffness (*SI Appendix*, Fig. S4), showing the importance of clustering migration in deeper mechanosensing underneath >100 μm. For the cell clusters on collagen layers with stiffer basal substrate, longer clustering phase and slower migration led to smaller number of dispersive cells compared to softer basal matrix (Fig. 2*F*). By contrast, in case of softer

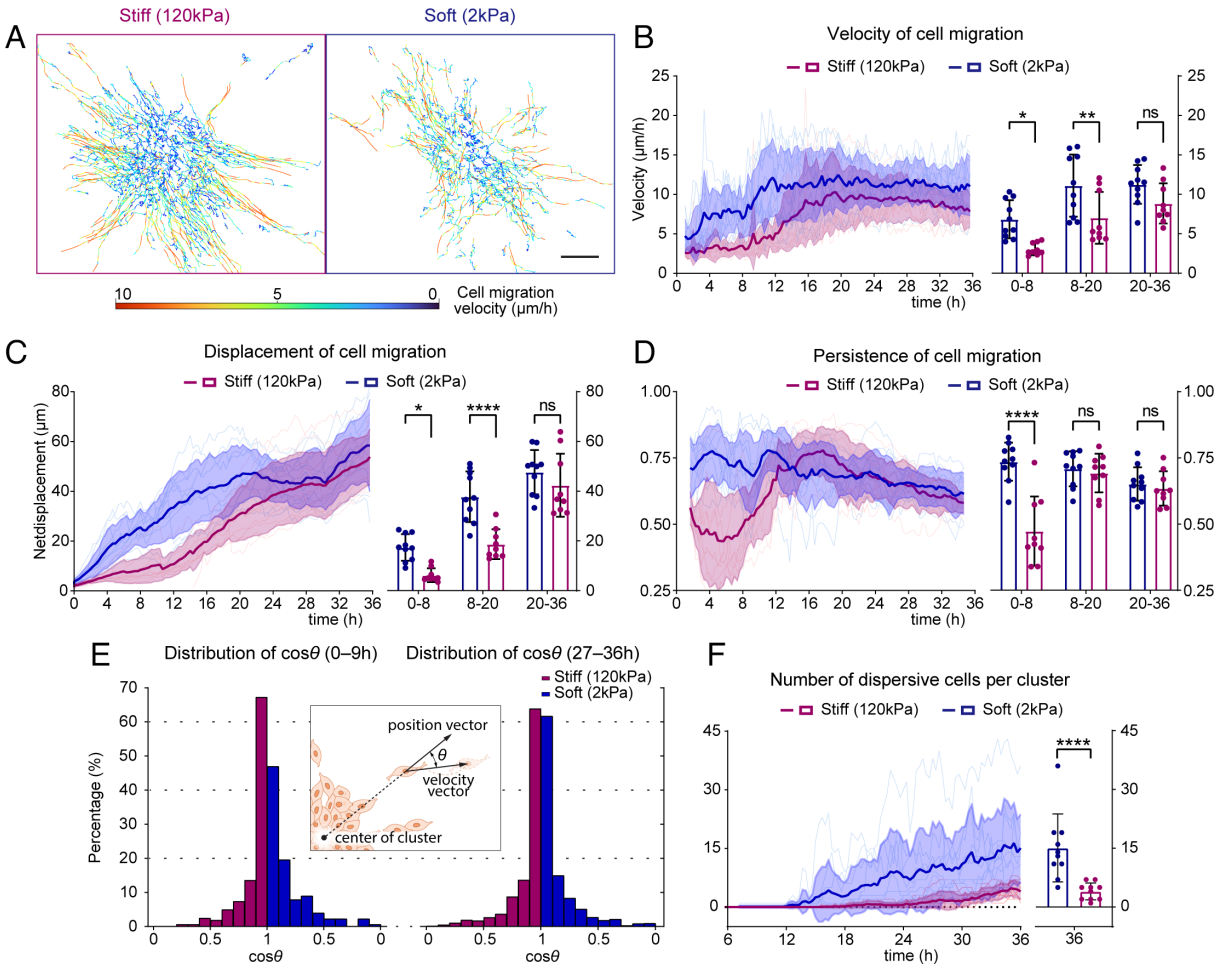

Fig. 2. Depth-mechanosensing of stiffer basal matrix limits dispersal of grouped epithelial cells. (*A*) Cell migration trajectories colored with real-time migration velocity. (Scale bar, 100 μm.) (*B–D*) Velocity, displacement, and persistence of cellular migration on col-PA substrate with different basal layer stiffness. Darker color indicates mean ± SD, while lighter color indicates the replicates. *P < 0.05, **P < 0.01, ****P < 0.0001, ns = not significant, two-way ANOVA. N = 10. (*E*) Schematic and histogram of the cosine of the angle θ (radial persistence) distribution on col-PA substrate with different stiffness. (*F*) Number of dispersive cells per cluster on col-PA substrate with different stiffness. ****P < 0.0001, Student's t test. N = 10.

basal substrate, number of dispersive cells per cluster steadily increased (Fig. 2*F*), and the cells no longer migrate collectively (Fig. 1 *C* and *D* and *SI Appendix*, Fig. S1*A* and Movie S1). These differences in cell clustering, migration, and dispersal between soft and stiff basal matrices underneath >100 μm thick collagen layer indicate deeper mechanosensing of epithelial clusters than previously shown for single cells (<10 μm) (16, 18, 19, 29, 30), indicating that "depth-mechanosensing" could be an emergent phenomenon enhanced by cell collectives.

Reduced Cell Dispersal Due to Depth-Mechanosensitive Collagen Deformation and Stiffening. According to previous studies, cellular clustering increases on softer matrices that generate lower forces, slower migration, and impart epithelial characteristics (26, 27). Contrary to this observation, on collagen-layered matrices, we observe that stiffer basal matrices slow cell migration and limit cell dispersal, thus promoting clustering (Figs. 1 and 2). Since our layered matrix system uses collagen as the adhered ECM that can be actively deformed and remodeled by cells, we sought to understand how collagen mechanics relates to the observed depth-mechanosensitive cell dispersal phenotypes (Fig. 3*A*). To quantify collagen deformation during cell clustering and migration, we incorporated fluorescence beads within collagen and tracked their movement over time in the 3D space around the epithelial clusters (Movies S1, *Bottom* and S2). We found higher displacement of beads embedded in collagen attached to stiffer basal matrix (Fig. 3*B*). In both soft and stiff groups, collagen bead displacements were directed toward the center of the epithelial cluster, indicating that cell contractility pulls collagen fibers (*SI Appendix*, Fig. S8*A*, with vectors showing inward direction) and this contraction is higher in case of stiffer basal matrix.

When tracked over time, velocity of collagen displacement on stiff basal matrix increased and peaked over the first 12 h (Fig. 3*C*), consistent with the duration of clustering phase noted above (Fig. 1). In comparison, on soft basal matrix, average velocity of collagen displacement peaked after ~8 h (Fig. 3*C*), also consistent with the clustering phase of this condition. Through these comparisons, we noted that cell migration speed increases (Fig. 2*B*) after peak velocity of collagen deformation is attained (around ~8 h for soft and ~12 h for stiff; Fig. 3*C*). These seemingly segregated phases of collagen deformation and cell migration suggest that contractile cellular forces first perform collagen deformation and then cellular protrusions use the deformed collagen to migrate. We also found that the persistence of collagen deformation remained high during the first clustering phase (<8 h for soft and <12 h for stiff) and subsequently reduced during the cell migration phase (Fig. 3*E*). Thus, the phases of high velocity of collagen deformation and cell migration do not overlap, and cell migration ensues after adequate collagen deformation has occurred. During the cell migration phase (>12 h), although the velocity of collagen deformation reduced in both conditions, it remained higher for the stiffer basal matrix (Fig. 3 *C* and *D*). As a result, the net displacement of collagen deformation, measured as the average displacement of collagen beads, was higher on stiffer basal matrix throughout the migration phase (Fig. 3 *C*–*E*). These findings indicate that greater collagen contraction, enabled here by the stiffer basal matrix, promotes clustering and limits dispersal of epithelial collectives. Conversely, a softer basal matrix lacks coordinated collagen deformation, which allows random dispersal of cells out of the epithelial collective before adequate cell clustering can occur.

Next, we asked whether these depth-mechanosensitive changes in collagen deformation alter the mechanical properties of the collagen matrix around epithelial collectives that could explain the observed differences in cell dispersal phenotypes. According to reflectance and two-photon excitation images, collagen structure underneath the cell cluster undergoes higher remodeling in the case of stiffer basal matrix (*SI Appendix*, Figs. S6 and S10). To understand whether these visual observations are associated with changes in collagen stiffness in different regions relative to cell clusters, we performed atomic force microscopy (AFM) in the front and side areas around epithelial streams (Fig. 3*G* and *SI Appendix*, Fig. S7). We found that collagen stiffness in front of epithelial streams was significantly higher with stiffer basal matrix (Fig. 3*H*, comparing regions *a* versus *c* in Fig. 3*G*). However, in the side regions around epithelial streams, collagen stiffness was lower and did not change between the two groups (Fig. 3*H*, regions *b* versus *d* in Fig. 3*G*). These differences in collagen stiffness in the front and side areas suggest that epithelial clusters generate radially inward collagen contraction as they migrate outward, which is also consistent with the collagen deformation mapping results (Fig. 3*B* and *SI Appendix*, Fig. S8*A*). For the cell clusters with stiffer basal substrate in depth, higher collagen stiffening (Fig. 3 *G* and *H*) and deformation (Fig. 3 *B*–*D*) allow cells to sense the stiff basal matrix and exhibit higher contractility, which builds up positive feedback and further enhances the depth-sensing.

Since "depth-mechanosensing" requires that cell-generated matrix deformation propagate deep through the collagen layer to the basal PA gel surface, we tracked collagen displacement in the 3D space around epithelial clusters (Fig. 3*F* and *SI Appendix*, Fig. S9*A*). We found that collagen gel underneath the cell cluster became thinner over time while generating inward collagen deformation, which results in a basin-like shape of collagen gel around the cells (Fig. 3*F* and *SI Appendix*, Fig. S8*B*). To test the propagating depth of cell-generated deformation, we also repeated experiments on double-layer substrates with a thicker collagen layer (~300 μm, *SI Appendix*, Fig. S9*B*) and found that cell-generated collagen deformation dissipated over distance (*SI Appendix*, Fig. S9*B*), and the difference between cell cluster migration with different basal PA gel stiffness also simultaneously decreased (*SI Appendix*, Fig. S5 *I*–*L*). According to these observations, cell clusters can deform collagen matrices both in horizontal and vertical directions on double-layer substrates, and cellular depth-mechanosensing of the stiffer basal layer could occur through this spatially coordinated 3D collagen deformation (Fig. 3).

To address the importance of the collagen layer in depth-mechanosensing, we also patterned the cell clusters on collagen-coated PA gel with different stiffness instead of the collagen-PA double-layer substrates. Upon removal of the collagen layer altogether, epithelial cells dispersed without clustering regardless of ECM stiffness (*SI Appendix*, Fig. S5*A*), indicating that collagen deformation around epithelial colonies enables their clustering. The cell clusters on the collagen coating PA gel have higher cell migration velocity (*SI Appendix*, Fig. S5 *B*–*D*), which is opposite to the double-layer substrate results wherein MCF10A cell clusters with softer basal PA layer undergo dispersal with higher cell migration velocity while those with depth-mechanosensing of stiffer basal layer undergo clustering (Fig. 2 *A*–*D*). We also repeated experiments for higher collagen density 2.0 mg/ml with a Young's modulus ~500 Pa compared to the ~200 Pa 1.3 mg/ml controls above (*SI Appendix*, Fig. S2*B*), and found cell dispersal in both conditions (*SI Appendix*, Fig. S5*E*), indicating that denser collagen hampers propagation of ECM deformation (*SI Appendix*, Fig. S9*D*) and blocks sensing of basal matrix stiffness (*SI Appendix*, Fig. S5 *F*–*H*). The lack of depth-mechanosensing in single-cell experiments (*SI Appendix*, Fig. S4) could also be explained by their lower ability to deform collagen (*SI Appendix*, Fig. S9*C*). Overall, these findings (Figs. 1–3) suggest that an active coupling between contractility-driven collagen deformation and cell migration regulates depth-mechanosensitive epithelial clustering and dispersal.

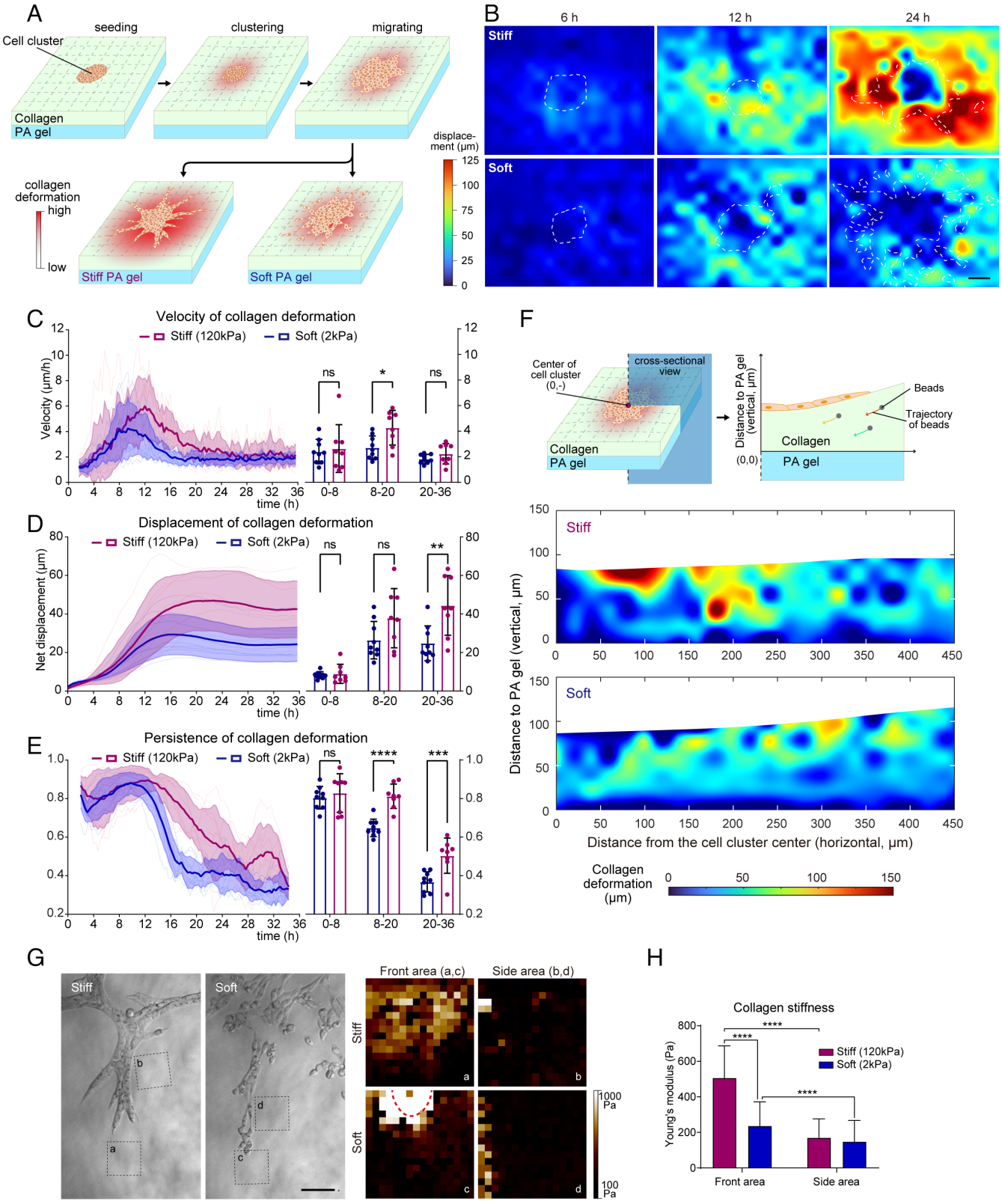

Fig. 3. Collagen deformation and stiffening during depth-mechanosensing of cell clusters. (*A*) Schematic of cell cluster induced collagen deformation on collagen-PA double-layer substrate with different PA gel stiffness. (*B*) Heatmap of collagen deformation. (Scale bar, 100 μm.) (*C*–*E*) Velocity, displacement, and persistence of beads labeled collagen deformation on col-PA substrate with different basal layer stiffness. Darker color indicates mean ± SD, while lighter color indicates the replicates. N = 10. (*F*) Cross-sectional projection view of collagen displacement in 3D. Colored with collagen deformation in 3D. (*G*) Mapping of collagen stiffness on the leading edge of the cluster (*A* and *C*) on the side of it (*B* and *D*). 6.25 μm × 6.25 μm per pixel in the heatmap. (Scale bar, 100 μm.) (*H*) Collagen stiffness in different areas on the leading edge of clusters. N > 10. *P < 0.05, **P < 0.01, ***P < 0.001, ****P < 0.0001, ns = not significant, two-way ANOVA.

Cell-Populated Collagen-PA Double-Layer Model Captures Depth-Mechanosensitive Cell Clustering and Dispersal. Our experimental findings suggest a complex interplay of cell contractility, collagen fiber deformation, 3D propagation of collagen deformation, feedback from the basal matrix, and multicellular coordination to enable the observed depth-mechanosensitive epithelial clustering

and dispersal. We wondered whether this convolution of parameters could be simplified into a physically consistent set of rules that could explain the observed behavior, and whether such a model could make new testable predictions. In that attempt, we adopted and modified a double-layer computational model of cell–collagen interactions from previous work (31, 32), as detailed in the Methods section and in *SI Appendix*, Fig. S16. Briefly, our modified cell-populated collagen-PA (CPCP) double-layer model is composed of triangular spring-based lattice to capture the collagen fiber network, which is connected to nodes that make up the cells, and these collagen elements are connected to a layer of linear elastic basal matrix (PA gel in experiments) that is separately modeled in a finite elements framework (Fig. 4 *A* and *B*). In our reductionist system, the cellular behavior is governed by four independent parameters corresponding to adhesions, migration, protrusions, and contractility, which are proportional to a mechanosensing signal at each cell node (Fig. 4*A* and *SI Appendix*, Fig. S17 *A–C*; detailed description in Methods and *SI Appendix*, Fig. S16). In this CPCP model, depth-mechanosensing is realized by linking adhesion sites of cells to PA substrates through collagen networks (Fig. 4*B*). As such, cellular contractile forces deform the spring-based collagen elements, which in turn deform the PA layer. By measuring the change of the remaining force within intermediate collagen networks (Eq. **3**), cells could sense the depth-mechanosensing feedback from the basal layer (PA substrates) without direct contact and change their behavior accordingly.

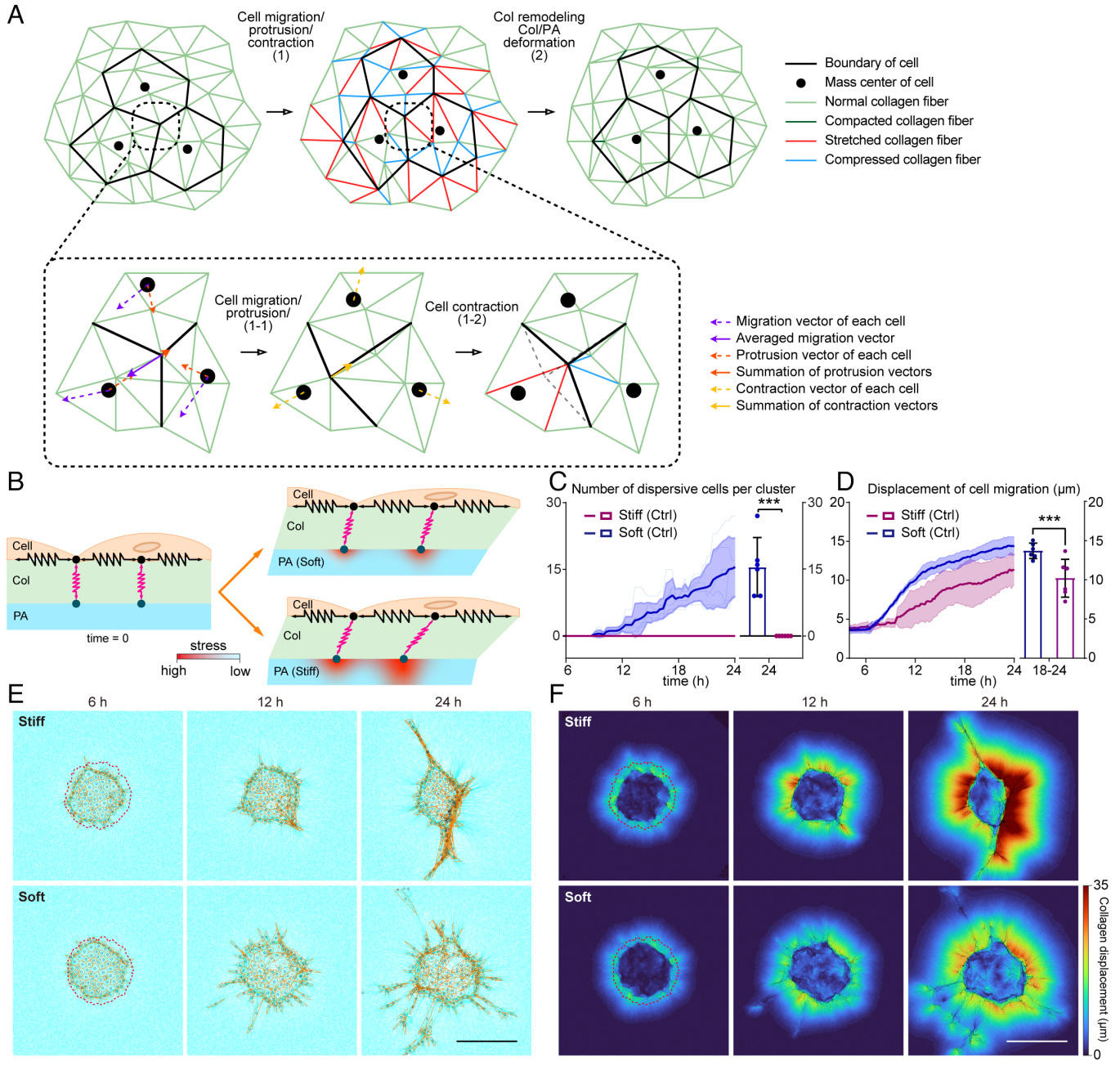

Fig. 4. Depth-mechanosensitive cell clustering and dispersal in cell-populated collagen-PA double-layer model. (*A* and *B*) Schematic of the Cell-Populated Collagen-PA (CPCP) mathematical model, while red color indicates the stress within PA gel. (*C*) Number of dispersive cells per cluster on CPCP mathematical model with different basal layer stiffness. (*D*) Net displacement of cell migration on CPCP mathematical model with different basal gel stiffness. Data are expressed as mean ± SD, N = 6. ***$P < 0.001$, Student's *t* test. (*E*) Cell cluster formation in CPCP model. The orange polygon indicates the cell shape, the black circle indicates the mass center of the cell, cyan lines indicate the collagen network, the red dashed line indicates the initial shape of cell clusters. (*F*) Collagen deformation in the CPCP model with different PA gel stiffness. (Scale bar, 100 μm.)

We started simulations with a constant cellular contractile force for both soft and stiff basal matrices (PA layer), so as not to presume depth-mechanosensing. Given the equivalent force in both conditions, the stiffer PA gel underwent smaller deformation due to its linear elastic modulus, and a larger portion of matrix deformation occurred in the collagen network (Fig. 4*B*, depicted as magenta springs). By responding to this larger deformation in the collagen network via the mechanosensing signal, cells in the CPCP model could indirectly sense and respond to the stiffer basal PA layer, thus enabling depth-mechanosensing. We changed the stiffness of PA gel in the CPCP model (*SI Appendix*, Table S2) and simulated the response of cell groups in terms of their ability to perform collagen contraction, PA deformation, and cell migration. In the initial hours, as cells contracted collagen elements, cell cluster size decreased with a simultaneous rise in collagen deformation in both soft and stiff basal PA matrices (Fig. 4 *E* and *F*). In these simulations, cell migration velocity was lower for stiffer basal PA layer (Fig. 4*D* and *SI Appendix*, Fig. S18), which is consistent with our experimental measurement for analogous conditions (Fig. 2*B*). Over time, collagen deformation accumulated, to a greater extent in case of stiffer basal PA layer (Fig. 4*F*), and cells within the cluster contracted with higher deformation of collagen elements and formed finger-like processes at the edges (Fig. 4*E*). By contrast, cells in the collagen network connected to the softer basal PA layer ended up deforming the PA layer with lower contraction of the collagen elements, thus dispersing out of the collective more easily (Fig. 4 *E* and *F* and Movie S5). According to our reductionist model of spring-based collagen elements tied to continuum-based PA finite elements, cell-generated forces cause higher deformation in softer basal PA substrate (Fig. 4*B*), thus resulting in lower deformation in collagen element, loss of depth-mechanosensing, and increased cell dispersal. By contrast, lower deformation of stiffer basal substrate allows higher retention of force-based collagen deformation (Fig. 4*B*) and depth-mechanosensitive epithelial clustering.

Loss of Depth-Mechanosensing by Disrupting Coordinated Collagen Deformation Through α-Catenin Knockdown or Myosin Inhibition. According to our findings of emergent

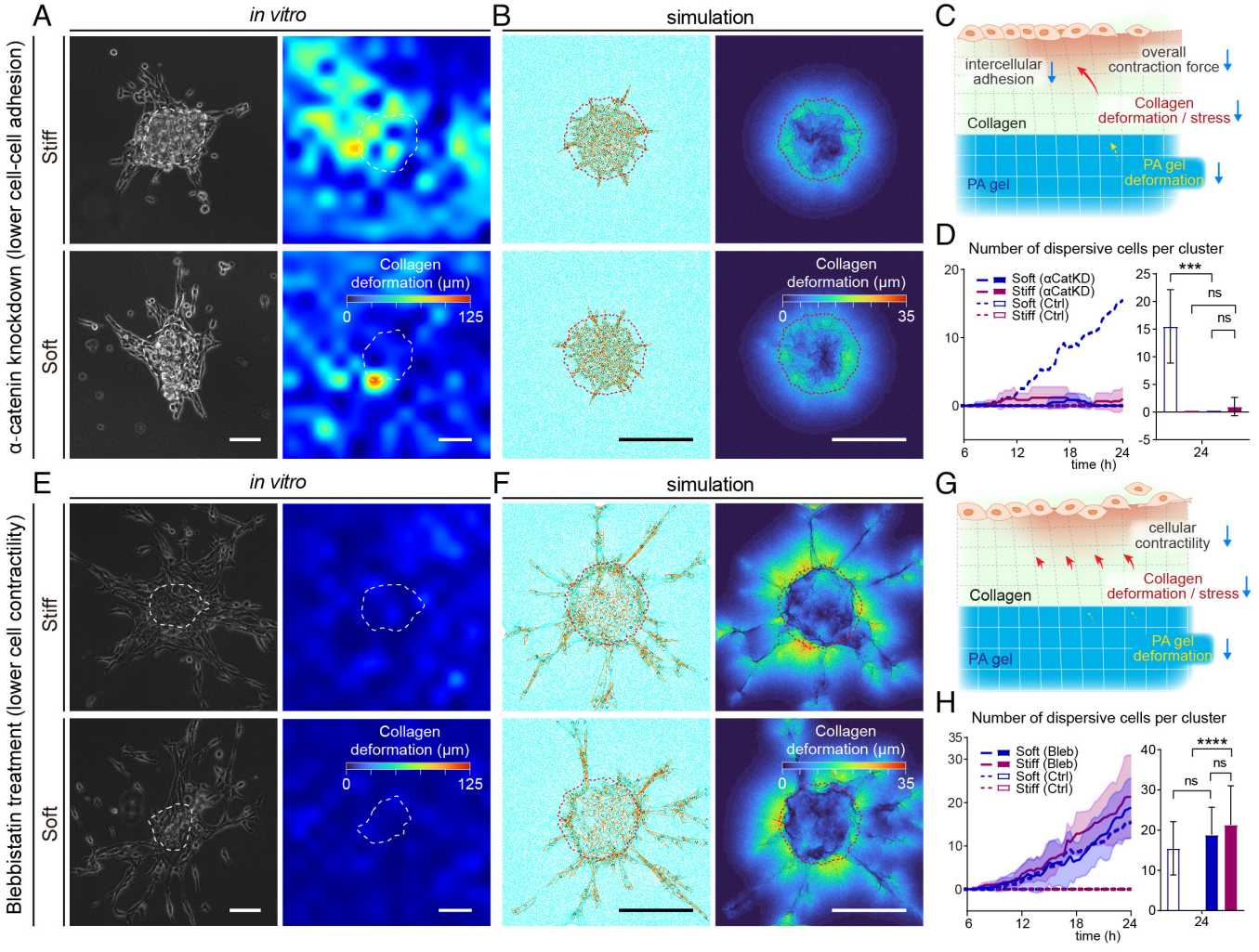

Fig. 5. Disrupting coordinated collagen deformation through α-catenin knockdown or myosin inhibition attenuates depth-mechanosensing. (*A*) Brightfield image of cell cluster formation, and heatmap of collagen deformation in α-catenin knockdown (αCatKD) MCF10A cells at 24 h in vitro. (*B*) Cell cluster formation and collagen deformation heatmap in CPCP model with less cell–cell interaction, mimicking the αCatKD cells. The orange polygon indicates the cell shape, the black circle indicates the mass center of the cell, cyan lines indicate the collagen network, the red dashed line indicates the initial shape of the cell clusters. (Scale bar, 100 μm.) (*C*) Schematic of cluster formation with α-catenin knockdown cells. (*D*) Number of dispersive cells per cluster in αCatKD cell clusters in vitro. N = 6. Data are expressed as mean ± SD. (*E*) Brightfield image of cell cluster formation, and heatmap of collagen deformation in blebbistatin (Bleb) treatment MCF10A cells at 24 h. (*F*) Cell cluster formation and collagen deformation heatmap in CPCP model with lower cellular contractility, mimicking the Bleb-treated cells. (Scale bar, 100 μm.) (*G*) Schematic of cluster formation with Bleb-treated cells. (*H*) Number of dispersive cells per cluster in Bleb-treated cell clusters in vitro. N = 6. Data are expressed as mean ± SD. ***$P < 0.001$, ****$P < 0.0001$, ns = not significant, two-way ANOVA.

depth-mechanosensing, epithelial collectives can sense deeper through the collagen layer, ~100 μm, as opposed to the previously shown depth-sensing of ~10 μm by single cells. Given the demonstrated importance of grouped cell contractility through modeling and experiments, we next asked whether loss of cell–cell interactions affects the observed cell clustering and dispersal. To that end, we repeated experiments with α-catenin knockdown (αCatKD) MCF10A cells to attenuate intercellular adhesion, as we have done previously (33), and they appeared to undergo similar phases of clustering and migration as the wildtype MCF10A cells (Fig. 5*A* and Movie S4). Although α-catenin depletion has been known to enhance epithelial cell motility in some previous studies (34), on our layered col-PA gels, αCatKD cells migrate more slowly than wild-type cells, and there is no significant difference between soft and stiff basal layers (Fig. 5*A* and *SI Appendix*, Figs. S11 *A* and *B* and S14*A*). Since α-catenin depletion is known to disrupt the collective migration and contractility of epithelial cells (34–36), the observed reduction in cell migration persistence and collagen deformation was expected (*SI Appendix*, Figs. S11*C* and S14*B*). However, despite lower intercellular adhesions after α-catenin knockdown, cell dispersal remained low (Fig. 5*D*) on both soft and stiff basal layers, indicating that lower collective collagen contraction due to the loss of intercellular coordination of αCatKD cells suppresses their migration. To understand whether loss of cell–cell adhesions could predict a similar response in our CPCP computational model, we performed simulations using a lower cell adhesion coefficient (*SI Appendix*, Table S2) and found a significant decrease in collagen deformation and cell migration (Fig. 5*B* and *SI Appendix*, Figs. S11*C*, and S18*F*). Simulations also showed loss of cell streaming at cluster edges and a reduced number of dispersive cells (Fig. 5*B* and *SI Appendix*, Fig. S11*F*, and Movie S6) on both soft and stiff basal layer cases. Overall, αCatKD cells showed lower collective collagen deformation, cell migration velocity, and number of dispersive cells on collagen gels with both soft and stiff basal layers, which resembled results with wildtype cells on softer col-PA gels, indicating no advantage from depth-mechanosensing. To verify the potential effect of epithelial–mesenchymal transition (EMT) in cell migration, we also imaged the vimentin expression of MCF10A cell clusters under different conditions (*SI Appendix*, Figs. S10 and S13). In both control and αCatKD groups, no significant difference between double-layer substrates with different basal layer stiffness was found, indicating that the EMT might not be the driving force of the depth-mechanosensing phenotypes.

Since the ability of cells to generate forces that propagate collagen deformation deep through the layers is central to depth-mechanosensing, we next sought to disrupt myosin activity and measure epithelial response. We treated MCF10A cells with blebbistatin and found rapid dispersal of the seeded epithelial colonies along with negligible collagen deformation (Fig. 5*E*) for both soft and stiff basal PA layers. Here, the initial phase of cell clustering and collagen deformation is dramatically reduced, and cells instead enter directly into the migration and dispersal phase on both soft and stiff basal layers (Fig. 5 *E* and H, and *SI Appendix*, Figs. S12 and S14*C*). As a result of the reduced collagen deformation (Fig. 5*E*, and *SI Appendix*, Figs. S12*C* and S15*C*), cell clusters become insensitive to the basal layer stiffness and instead become highly protrusive due to loss of myosin-based contractility and become highly migratory and dispersive (Fig. 5*E* and Movie S7). In our simulations using the CPCP model, lowering the cell contractility parameter yields the same results wherein collagen deformation is similar in both soft and stiff cases, and cells become highly dispersive (Fig. 5*F* and *SI Appendix*, Fig. S12 *E* and *F* and Movie S7), consistent with experimental results.

Discussion

Over the past two decades, a fundamental paradigm of cellular mechanosensing has emerged wherein cells transduce mechanical cues of their adhered extracellular surfaces through receptor–ligand bonds and actin–myosin forces (8, 10). The resulting mechanotransduction signaling regulates a variety of cellular responses, including differentiation, growth, and migration. In mechanical dynamic microenvironments of developing embryos, cells can generate their own mechanical environment and undergo durotaxis to migrate along the stiffness gradients (37). In addition to sensing the stiffness of their current ECM, migrating cells can remember the stiffness of their past environments through a stored mechanical memory (33, 38). Given this emerging evidence of the ability of cells to mechanosense beyond their current ECM, we wondered whether cells could respond to stiffer environments away from their immediately adhered ECM. One analogy could be the difference in sensory perception of sleeping on a mattress that is lying on a floor versus the same placed on a bed frame. Since ECM deformation generated by cellular forces regulates mechanosensing, such ECM deformations could travel through deeper ECM layers, and the cells could thus sense stiffness beyond their immediately adhered surface. This is an important yet overlooked aspect of cellular mechanosensing in physically complex microenvironments, because cells reside in multilayered tissue contexts

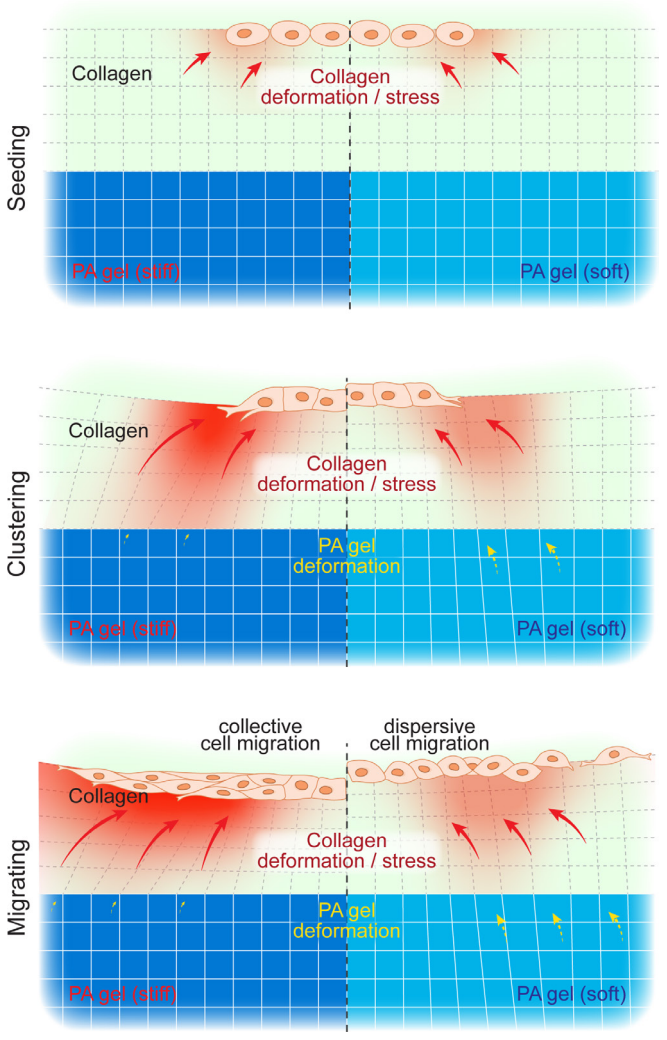

Fig. 6. Schematic of cell clustering and dispersal on collagen-PA double-layer substrate with different basal layer stiffness.

such as the basement membrane attached to interstitial tissue and the tumor–stromal interface between the stiff tumor and softer healthy adjacent tissue.

To understand the depth-mechanosensing of epithelial collectives in the presence of physically heterogeneous multilayered matrices, we developed an in vitro collagen-polyacrylamide (PA) double-layer system for cell culture. We find that epithelial collectives could sense the distant stiff matrices over 100 μm, showing as enhanced clustering and reduced cell migration. Through a cell-populated collagen-PA (CPCP) double-layer mathematical model, we delineate how depth-mechanosensing arises from cell contractility, collagen deformation, and multicellular coordination in different matrix layers. These findings expand the known length scales of cellular depth-mechanosensing to >100 μm, which was previously shown to be <5 μm for linear elastic matrices (16) and ~10 μm for collagen matrices (21) with single cells. Although there is prior work showing that a group of cells deform their ECM to a greater extent than single cells (39–41), the functional advantages of enhanced "collective deformation" of the ECM for cell collectives have not been demonstrated. Additionally, the impact of these forces when they reach long distances and encounter different matrix interfaces, as well as whether cell groups can sense these distant interfaces, is poorly understood. Here, using our double-layer system, we show a functional role for long-distance force transmission in depth-mechanosensing by the collective contractility of epithelial cells. The collective ECM deformation generated by epithelial cells extends the range of cellular depth-sensing from a few microns to tens of microns, which in turn alters cellular phenotypes in their dispersal and clustering due to depth-mechanosensing of basal substrates (Fig. 6). Since the ECM stiffness in vivo is highly heterogeneous, with significant differences across length scales of a few cells (12, 42), the depth-sensing of cell clusters on fibrous matrices across tens of cells in distance could play an important role in morphogenesis and disease progression.

When cells directly adhere to the bulk matrices, the substrate stiffness is shown to affect the intercellular contacts in epithelial cells, where softer substrates lead to cell clustering and stiffer substrates cause dispersal (18, 19). In addition, on our collagen-PA double-layer system, cell clusters on the stiffer basal layer show significant clustering and collective migration, while clusters on the softer basal layer tend to migrate in a dispersive manner. Evidenced by the simulation results in our CPCP model, we attribute the aforementioned difference in stiffness response to the intercellular cooperation within cell clusters and the feedback from the fibrous matrix with heterogeneous stiffness. When seeded on a fibrous matrix, such as collagen, cells in the clusters could apply a higher contractile force compared with single cells, and thus sense and respond to the stiffness change in the distant substrate. For the cell clusters with a stiffer substrate at a distance, cells will assume that they are on a stiff matrix and exhibit higher contractility, which builds up positive feedback and further enhances the depth-sensing. In future work, to further understand the long-range depth-sensing of epithelial collectives on fibrous matrices with varying structural and geometrical properties (e.g., prealigned, different fiber length and width) and protein composition (e.g., collagen IV, laminin) should be verified to mimic the in *vivo* biomechanical environment. In addition, understanding collective depth-mechanosensing for different cell types from varying disease states and animal contexts will broaden our understanding of the cellular dynamics during tumor growth, organ formation, and disease propagation.

Methods

Layered Collagen-Polyacrylamide (col-PA) Gel Fabrication. Polyacrylamide (PA) gels with varying stiffness were made by mixing different percentages of acrylamide: bis-acrylamide in H_2O [for 2 kPa PA-gel, 4%:0.2%, for 120 kPa PA-gel, 15%:1.2%, stiffness verified by AFM (*SI Appendix*, Fig. S2)]. Ammonium persulfate (APS, 0.5 μg/ml) and N-N′-N-N′-tetramethyl ethylenediamine (TEMED, 0.5 μl/ml) were added to the precursor solution after degassing and allowed to fully polymerize on the activated glass surface for 30 min. PA gels were rinsed and stored at 4 °C in PBS. Before layering collagen gels, PA gels were sterilized by ultraviolet light for 1 h and treated with 0.5 mg/ml Sulfo-SANPAH solution (Thermo Fisher) to allow the attachment of collagen. Rat-tail collagen type I (Advanced Biomatrix) solution was diluted to a concentration of 1.3 mg/ml with culture medium and adjusted to a pH of ~7.2 with 1 M NaOH. The collagen precursor solution was added on top of the activated PA gel surface and then cultured at 37 °C for 30 min to allow gelation. For visualization of collagen deformation, fluorescent microbeads (carboxylate-modified microspheres, 1 μm in diameter, 540/560 nm, Invitrogen) were added to the precursor solution (0.1% (v/v)) in the samples prepared for collagen deformation analysis. For the collagen-coated PA gel group, after Sulfo-SANPAH treatment, instead of fabricating collagen hydrogel, PA gel substrates were incubated with 0.05 mg/mL collagen solution at 4 °C overnight, followed by a washing step to remove unattached collagen proteins.

Multi-Cell Cluster Patterning on the col-PA Substrate. Photo-crosslinkable PA-gel was used to fabricate the defined geometries (Fig. 1*A*). Here, PA solution amenable to be crosslinked by UV exposure (15% acrylamide, 1.2% bis-acrylamide and 7.5 mg/ml irgacure 2959) were coated to a thickness of 200 μm and exposed to 365 nm UV light through a photomask with defined geometries. Microwells with diameters from 100–500 μm were tested. Polydimethylsiloxane (PDMS) molds were fabricated by polymerizing on the photo-crosslinkable PA-gel mold. PDMS pre-polymer solution was prepared by mixing base and curing agents of Sylgard 184 Silicone Elastomer (Dow Corning, Midland, MI) in 10:1 weight ratio. MCF10A cells were patterned on the collagen-PA substrate by adopting a previous protocol (43), as illustrated in Fig. 1*A*. MCF10A cells were trapped in the microwells (~200 μm diameter, ~150 μm depth, wells separated by 2 mm) on the PDMS chamber (length and width of 2 cm, Fig. 1*A*) before collagen gelation. Cell clusters were formed on collagen gels after the PDMS chamber was removed. In the collagen-coated PA gel group, the same cell patterning method was applied, while the collagen gel solution was replaced by cell culture medium.

Cell Culture and Live Imaging. Human mammary MCF-10A epithelial cells were cultured in DMEM/F12 (Invitrogen) supplemented with 5% (v/v) horse serum (Invitrogen), 20 ng/mL epidermal growth factor (EGF, Miltenyi Biotec Inc), 0.5 mg/mL hydrocortisone (Sigma-Aldrich), 100 ng/mL cholera toxin (Sigma-Aldrich), 10 μg/mL insulin (Sigma-Aldrich), and 0.1% (v/v) Normocin antibacterial, antifungal, and antimycoplasma cell media supplement (Invivogen), as previously described (44). MDCK I, A431, breast cancer-derived cancer-associated fibroblasts (CAFs) were cultured in DMEM (Invitrogen) supplemented with 10% (v/v) fetal bovine serum (Gibco), and 0.1% (v/v) Normocin. α-catenin knockdown (αCatKD) MCF-10A cell line was used in the αCatKD group. In the blebbistatin (Bleb) group, cells were treated with 2 μM blebbistatin after cell seeding. For live timelapse imaging, cells were transferred to a Zeiss Cell Observer inverted microscope (Carl Zeiss Microscopy, Germany) with a live-imaging system and were tracked for 36 h (z-stacks with 6 μm intervals were acquired every 20 min). ImageJ (NIH) with TrackMate 7 (45) plugin was used to analyze cell migration. Persistence in migration refers to a cell's tendency to maintain its direction of movement rather than changing direction abruptly. Linear persistence is calculated as the displacement divided by the total distance traveled over 4 h. Radial persistence is calculated as the cosine of the angle between position vector and cell migration velocity vector (Fig. 2*E*). As illustrated in *SI Appendix*, Fig. S19, radial persistence could be a more appropriate measure of persistence than the linear persistence in case of circular cell clusters that migrate in radially outward direction.

AFM. Stiffness mapping of collagen around epithelial cells was performed using a Bruker Nanoscope Resolve Atomic Force Microscope (Bruker, Billerica) mounted on an inverted fluorescence microscope (Zeiss Observer A1 stand). Silicon nitride cantilever with a polystyrene bead (4.5 μm in diameter) attached at the tip (Novascan Technologies, Inc., Boone, IA) with a nominal spring constant of 0.01 N/m was used

for operating force measurement. Data analysis was implemented in Nanoscope Analysis Software (Bruker, Billerica, USA) using a modified Hertz model.

Immunofluorescent Staining and Imaging. Cells for immunofluorescence imaging were fixed in 4% paraformaldehyde solution for 15 min, washed with DPBS, and permeabilized with 0.1% solution of Triton X-100 (Santa Cruz) for 1 h after 36 h of culture. After incubation with blocking buffer (DPBS with 1% bovine serum albumin and 10% goat serum) for 1 h at room temperature, samples were incubated overnight at 4 °C with primary antibodies. Samples were washed, incubated with secondary antibodies for 1 h 45 min at room temperature, and washed again in DPBS. For actin visualization, samples were incubated with phalloidin (1:300, Invitrogen) for 30 min and washed with DPBS. Fluorescent images of cell clusters and reflection images of collagen were taken using the confocal microscope (Zeiss LSM 880, Carl Zeiss Microscopy, Germany) using 20x and 40x objectives. Two-photon excitation collagen imaging was performed with an LSM 880 (Zeiss, Germany) equipped with a Chameleon Discovery Ti:Sapphire laser (Coherent, Santa Clara, CA), where an 800 nm excitation wavelength was employed, and the emission was detected through the 520 nm bandpass filter.

Cell-Populated Collagen-PA (CPCP) Double-Layer Computational Model. To understand the roles of cellular adhesion, contractility, and motility in depth-sensitive epithelial cell clustering, a cell-populated collagen-PA (CPCP) double-layer model was adopted and modified from previous research (31, 32). The numerical computation and visualization for the model were accomplished in MATLAB (R2021a) (detailed schematic and description of this model is provided in *SI Appendix*, Fig. S16, and the source code is available on *Github*). In this model, cells are meshed on the col-PA double-layer matrices (Fig. 4*A* and *SI Appendix*, Fig. S16). Each cell is defined as a set of nodes that are directly attached to the collagen lattice nodes, with three individual parameters respectively to describe its migration, protrusion, and contraction, and one collective parameter to describe the cell–cell interaction. The collagen fiber network is defined as triangulated spring lattices that are linked to the polyacrylamide layer through the intermediate springs located at the lattice nodes (Fig. 4*A* and *SI Appendix*, Fig. S16). As cells deform and remodel the collagen lattices, the intermediate springs transfer the cell-generated force to the PA layer (Fig. 4*B* and *SI Appendix*, Fig. S16). The PA gel layer is described using a linear 2D finite element model (46). In this CPCP model, the cellular behavior on the Col-PA matrix is broadly divided into four steps:(Fig. 6)

1) *Migration and protrusion of cells.* Any cell node could move along the collagen lattices and find a new collagen lattice node to attach. The direction and magnitude of cell node movement are determined by its position and migration/protrusion parameters of the corresponding cell (or cells).
2) *Contraction.* Cells deform the collagen lattices by moving the collagen lattice nodes along with the attached cell nodes. The direction and magnitude of nodal movement are determined by the associated nodal position and contraction parameters. For instance, as illustrated in Fig. 4*A*, a given cell node (black) is attached to a collagen lattice node (green) and shared by three adjacent cells. Each cell has three individual displacement vectors due to migration, protrusion, and contraction whose magnitudes are directly proportional to their corresponding biochemical signaling parameters that vary with cells. The direction of migration vector is calculated using the orientation tensor of the collagen network (47) and position vectors of adjacent cells. The protrusion vectors are directed outward relative to the cell body, along the line connecting from the cell's center of mass to the given node; the contraction vectors are oriented in the opposite direction, toward the cell center. Cell–cell interaction is regulated by a binding coefficient shared within the same cell cluster. Cell proliferation was achieved by enabling the division of cells with the largest area.

$$\gamma v_{y_i} = F_i = \sum_j f_{i,j} + p_i, \qquad [1]$$

$$f_{i,j} = \begin{cases} 0, & d_{i,j} \le l_{i,j} \text{ and } f_{i,j} \text{ is normal} \quad (2.1) \\ -\Delta_\beta \beta \left(d_{i,j} - \Delta_l l_{i,j}\right) \dfrac{y_i - y_j}{d_{i,j}} \delta_{i,j}, & \text{if } f_{i,j} \text{ is compacted} \quad (2.2) \\ -\beta \left(d_{i,j} - l_{i,j}\right) \dfrac{y_i - y_j}{d_{i,j}} \delta_{i,j}, & d_{i,j} > l_{i,j} \text{ and } f_{i,j} \text{ is normal} \quad (2.3) \end{cases}, \qquad [2]$$

$$p_i = -\beta \left(1 - \frac{h_0}{\sqrt{{h_0}^2 + \left(y_i - z_i\right)^2}}\right)\left(y_i - z_i\right), \qquad [3]$$

$$d_{i,j} = \left\| y_i - y_j \right\|. \qquad [4]$$

3) *Collagen deformation.* Collagen lattices are deformed and remodeled by the cells, as described above, to reach a steady state. Eq. **1** describes the motion for the collagen lattice node i, where $f_{i,j}$ describes the force due to lattice entanglement and p_i describes the force generated by the PA gel. y_i is the location in R^2 of the collagen lattice node, v_{y_i} represents the velocity of y_i, and γ is the drag coefficient of the collagen lattice. Normal collagen fibers undergo stretching in a spring-like fashion (Eq. **2.3**) and remain unstressed under compression (Eq. **2.1**), with forces proportional to the level of stretching. In this spring-like behavior, $l_{i,j}$ is the spring initial length between two linked nodes i and j, and β is the spring constant of the collagen fibers. Compaction of fibers is a nonreversible part of collagen remodeling induced by cells. The spring constant of compacted fibers increases according to the coefficient Δ_β, and the spring initial length is reset to $\Delta_l l_{i,j}$. Compacted fibers resist compression as described in Equation (Eq. **2.2**). Since $f_{i,j}$ is only available when node i and node j are linked, the $\delta_{i,j}$ in (Eqs. **2.2** and **2.3**) indicates the link status, which is equal to 1 when node i and node j are linked and equal to 0 otherwise. At the beginning of the simulation, all collagen fibers start as normal (i.e., not compacted) and get remodeled to compacted status when the distance between two linked nodes ($d_{i,j}$) becomes short enough ($d_{i,j} \le \Delta_l l_{i,j}$) driven by cellular contraction. Node locations z_j are within R^2 region of the adhesion site of collagen on the PA gel surface, while the initial thickness of the collagen layer is h_0. When y_i and z_i have the same initial value, force in col-PA intermediate springs $\|p_i\| = 0$ is set at t_0, which subsequently increases with mismatch of deformations in collagen and PA gels. These variables and parameters are listed and described in *SI Appendix*, Table S1.

$$\sigma_i(t) = \frac{\sum_{t-\Delta t}^{t} {p_i(t)}'}{\Delta t} \quad \text{where} \quad {p_i(t)}' = \frac{\partial\left(p_i(t)\right)}{\partial\left(y_i\right)}. \qquad [5]$$

4) *PA deformation and stiff sensing.* The intermediate springs that connect collagen and PA layers transmit cellular forces to the PA layer through the collagen lattices (Fig. 4*B*). Deformation of the PA layer is calculated with a linear 2D finite element solver (46), using the same triangular mesh as the collagen lattices. The depth-mechanosensing of cells is implemented by measuring the depth-sensing parameter (σ) as shown in Eq. **5**. ${p_i(t)}'$ is the derivative of the remaining force within intermediate springs (p_i, shown in Eq. **3**) versus its displacement in the horizontal plane. $\sigma_i(t)$ is the depth-sensing parameter of the node i at time t, which is defined as the average of ${p_i(t)}'$ over time (Δt). Δt is 30 min in all the simulations. As shown in Fig. 4*B*, a stiffer PA layer undergoes smaller deformation, which leaves higher remnant force within intermediate springs, causing higher depth-mechanosensing feedback. This depth-sensing parameter (σ) directly influences the migration, protrusion, and contraction parameters of the corresponding cell.

Statistical Analysis. Statistical significance analysis was performed in GraphPad Prism 9, using two-way ANOVA following Tukey's multiple comparisons test or unpaired, two-tailed Student's *t* test.

Data, Materials, and Software Availability. The source code for building CPCP contraction model (MATLAB license required) and a high-resolution version of the visual description of the model (*SI Appendix*, Fig. S16) are freely available at: https://doi.org/10.5281/zenodo.16968126 (48). All study data are included in the article and/or supporting information.

ACKNOWLEDGMENTS. We acknowledge Washington University Center for Cellular Imaging (WUCCI) for two-photon confocal microscopy. We acknowledge financial support from following sources: NIH Grant R35GM128764 (to A.P.) and NSF, Civil, Mechanical and Manufacturing Innovation (CMMI) Grant: 2209684 (to A.P.).

1. Y. Liu *et al.*, Morphogenesis beyond in vivo. *Nat. Rev. Phys.* **6**, 28–44 (2023).
2. M. N. Starodubtseva, Mechanical properties of cells and ageing. *Ageing Res. Rev.* **10**, 16–25 (2011).
3. P. A. Janmey, R. T. Miller, Mechanisms of mechanical signaling in development and disease. *J. Cell Sci.* **124**, 9–18 (2011).
4. S. Mascharak *et al.*, Modelling and targeting mechanical forces in organ fibrosis. *Nat. Rev. Bioeng.* **2**, 305–323 (2024).
5. B. Ladoux, R. M. Mège, Mechanobiology of collective cell behaviours. *Nat. Rev. Mol. Cell Biol.* **18**, 743–757 (2017).
6. R. S. Stowers *et al.*, Matrix stiffness induces a tumorigenic phenotype in mammary epithelium through changes in chromatin accessibility. *Nat. Biomed. Eng.* **3**, 1009–1019 (2019).
7. A. Saez, M. Ghibaudo, A. Buguin, P. Silberzan, B. Ladoux, Rigidity-driven growth and migration of epithelial cells on microstructured anisotropic substrates. *Proc. Natl. Acad. Sci. U.S.A.* **104**, 8281–8286 (2007).
8. D. E. Discher, P. Janmey, Y. Wang, Tissue cells feel and respond to the stiffness of their substrate. *Science (80-)* **310**, 1139–1143 (2005).
9. R. J. Pelham, Y. L. Wang, Cell locomotion and focal adhesions are regulated by substrate flexibility. *Proc. Natl. Acad. Sci. U.S.A.* **94**, 13661–13665 (1997).
10. P. A. Janmey, D. A. Fletcher, C. A. Reinhart-King, Stiffness sensing by cells. *Physiol. Rev.* **100**, 695–724 (2020).
11. P. Ringer, G. Colo, R. Fässler, C. Grashoff, Sensing the mechano-chemical properties of the extracellular matrix. *Matrix Biol.* **64**, 6–16 (2017).
12. I. Acerbi *et al.*, Human breast cancer invasion and aggression correlates with ECM stiffening and immune cell infiltration. *Integr. Biol.* **7**, 1120–1134 (2015).
13. M. Tian *et al.*, The nanomechanical signature of liver cancer tissues and its molecular origin. *Nanoscale* **7**, 12998–13010 (2015).
14. C. Leclech, C. F. Natale, A. I. Barakat, The basement membrane as a structured surface–Role in vascular health and disease. *J. Cell Sci.* **133**, jcs239889 (2021).
15. J. Sodek, M. D. McKee, Molecular and cellular biology of alveolar bone. *Periodontol.* **2000**, 99–126 (2000).
16. S. Sen, A. J. Engler, D. E. Discher, Matrix strains induced by cells: Computing how far cells can feel. *Cell. Mol. Bioeng.* **2**, 39–48 (2009).
17. A. J. Engler, L. Richert, J. Y. Wong, C. Picart, D. E. Discher, Surface probe measurements of the elasticity of sectioned tissue, thin gels and polyelectrolyte multilayer films: Correlations between substrate stiffness and cell adhesion. *Surf. Sci.* **570**, 142–154 (2004).
18. A. Buxboim, I. L. Ivanovska, D. E. Discher, Matrix elasticity, cytoskeletal forces and physics of the nucleus: How deeply do cells "feel" outside and in?. *J. Cell Sci.* **123**, 297–308 (2010).
19. W. S. Leong *et al.*, Thickness sensing of hMSCs on collagen gel directs stem cell fate. *Biochem. Biophys. Res. Commun.* **401**, 287–292 (2010).
20. D. Wei *et al.*, Dynamically modulated core-shell microfibers to study the effect of depth sensing of matrix stiffness on stem cell fate. *ACS Appl. Mater. Interfaces* **13**, 37997–38006 (2021).
21. C. Walter, J. Mathur, A. Pathak, Reciprocal intra- and extra-cellular polarity enables deep mechanosensing through layered matrices. *Cell Rep.* **42**, 112362 (2023).
22. P. Friedl, D. Gilmour, Collective cell migration in morphogenesis, regeneration and cancer. *Nat. Rev. Mol. Cell Biol.* **10**, 445–457 (2009).
23. L. Li, Y. He, M. Zhao, J. Jiang, Collective cell migration: Implications for wound healing and cancer invasion. *Burn. Trauma* **1**, 21–26 (2013).
24. M. Vishwakarma *et al.*, Mechanical interactions among followers determine the emergence of leaders in migrating epithelial cell collectives. *Nat. Commun.* **9**, 3469 (2018).
25. A. M. J. Valencia *et al.*, Collective cancer cell invasion induced by coordinated contractile stresses. *Oncotarget* **6**, 43438–43451 (2015).
26. A. C. Brown, V. F. Fiore, T. A. Sulchek, T. H. Barker, Physical and chemical microenvironmental cues orthogonally control the degree and duration of fibrosis-associated epithelial-to-mesenchymal transitions. *J. Pathol.* **229**, 25–35 (2013).
27. S. C. Wei *et al.*, Matrix stiffness drives epithelial–mesenchymal transition and tumour metastasis through a TWIST1–G3BP2 mechanotransduction pathway. *Nat. Cell Biol.* **17**, 678–688 (2015).
28. S. Nasrollahi, A. Pathak, Topographic confinement of epithelial clusters induces epithelial-to-mesenchymal transition in compliant matrices. *Sci. Rep.* **6**, 18831 (2016).
29. B. Amnon, R. Karthikan, E. X. B. Andre, E. D. Dennis, How deeply cells feel: Methods for thin gels. *J. Phys. Condens. Matter.* **22**, 194116 (2010).
30. A. Buxboim, J. Swift, I. L. Ivanovska, J. Irianto, D. E. Discher, "How deeply cells feel?" in *Proc. IEEE Annu. Northeast Bioeng. Conf. NEBEC2014-Decem, 10–11* (2014).
31. J. C. Dallon, E. J. Evans, H. P. Ehrlich, A mathematical model of collagen lattice contraction. *J. R. Soc. Interface* **11**, 20140598 (2014).
32. L. Liu *et al.*, Matrix-transmitted paratensile signaling enables myofibroblast–fibroblast cross talk in fibrosis expansion. *Proc. Natl. Acad. Sci.* **117**, 10832–10838 (2020).
33. J. A. Almeida, J. Mathur, Y. L. Lee, B. Sarker, A. Pathak, Mechanically primed cells transfer memory to fibrous matrices for invasion across environments of distinct stiffness and dimensionality. *Mol. Biol. Cell* **34**, 490316 (2023).
34. E. N. Bunker, G. E. Wheeler, D. A. Chapnick, X. Liu, Suppression of α-catenin and adherens junctions enhances epithelial cell proliferation and motility via TACE-mediated TGF-α autocrine/paracrine signaling. *Mol. Biol. Cell* **32**, 348–361 (2021).
35. M. Takeichi, Multiple functions of α-catenin beyond cell adhesion regulation. *Curr. Opin. Cell Biol.* **54**, 24–29 (2018).
36. K. Matsuzawa, T. Himoto, Y. Mochizuki, J. Ikenouchi, A-catenin controls the anisotropy of force distribution at cell-cell junctions during collective cell migration. *Cell Rep.* **23**, 3447–3456 (2018).
37. A. Shellard, R. Mayor, Collective durotaxis along a self-generated stiffness gradient in vivo. *Nature* **600**, 690–694 (2021).
38. S. Nasrollahi *et al.*, Past matrix stiffness primes epithelial cells and regulates their future collective migration through a mechanical memory. *Biomaterials* **146**, 146–155 (2017).
39. J. Notbohm, J. H. Kim, A. R. Asthagiri, G. Ravichandran, Three-dimensional analysis of the effect of epidermal growth factor on cell-cell adhesion in epithelial cell clusters. *Biophys. J.* **102**, 1323–1330 (2012).
40. A. F. Mertz *et al.*, Scaling of traction forces with the size of cohesive cell colonies. *Phys. Rev. Lett.* **108**, 1–5 (2012).
41. C. G. Tusan *et al.*, Collective cell behavior in mechanosensing of substrate thickness. *Biophys. J.* **114**, 2743–2755 (2018).
42. R. Roy, J. P. Desai, Determination of mechanical properties of spatially heterogeneous breast tissue specimens using contact mode atomic force microscopy (AFM). *Ann. Biomed. Eng.* **42**, 1806–1822 (2014).
43. X. Gong, K. L. Mills, Large-scale patterning of single cells and cell clusters in hydrogels. *Sci. Rep.* **8**, 1–13 (2018).
44. S. Nasrollahi, A. Pathak, Topographic confinement of epithelial clusters induces epithelial-to-mesenchymal transition in compliant matrices. *Sci. Rep.* **6**, 18831 (2016).
45. D. Ershov *et al.*, Trackmate 7: Integrating state-of-the-art segmentation algorithms into tracking pipelines. *Nat. Methods* **19**, 829–832 (2022).
46. A.Al-Rumaithi, Linear 2D Finite Element Solver. MATLAB Central File Exchange. https://www.mathworks.com/matlabcentral/fileexchange/73189-linear-2d-finite-element-solver. Accessed 4 February 2022.
47. M. Aghvami, V. H. Barocas, E. A. Sander, Multiscale mechanical simulations of cell compacted collagen gels. *J. Biomech. Eng.* **135**, 1–9 (2013).
48. H. Yu, CPCP double-layer model (v1.0). Zenodo. https://doi.org/10.5281/zenodo.16968126. Deposited 14 November 2024.